ELSEVIER

Journal of Fluids and Structures 22 (2006) 541–555

JOURNAL OF FLUIDS AND STRUCTURES

www.elsevier.com/locate/jfs

Uniform-shear flow over a circular cylinder at low Reynolds numbers

S. Kang*

Department of Mechanical Engineering, Dong-A University, 840 Hadan2, Saha, Busan 604-714, Republic of Korea

Received 9 June 2005; accepted 7 February 2006
Available online 18 April 2006

Abstract

The present study has numerically investigated two-dimensional laminar flow over a circular cylinder with uniform planar shear, where the free-stream velocity varies linearly across the cylinder. Numerical simulations using the immersed-boundary method are performed for the ranges of $50 \leqslant \mathrm{Re} \leqslant 160$, $0 \leqslant K \leqslant 0.2$, and $B = 0.1$ and 0.05, where Re, K and B are the Reynolds number, the nondimensional shear rate and the blockage ratio, respectively. Results show that the flow depends significantly on the blockage ratio as well as the Reynolds number and shear rate. The vortex-shedding frequency and the mean drag remain nearly constant or slightly decrease with increasing shear rate. On the other hand, the mean lift is exerted from the side of the higher free-stream velocity to that of the lower one, and its magnitude increases linearly in proportion to the shear rate. Flow statistics as well as instantaneous flow fields are presented to identify the characteristics of the uniform-shear flow and then to understand the underlying mechanism.

Keywords: Blockage effect; Circular cylinder; Immersed-boundary method; Uniform-shear flow

1. Introduction

When the free-stream velocity exceeds a certain critical value in flow past a bluff body, vortex shedding occurs due to the flow instability in the near wake, resulting in periodically oscillating drag and lift forces. Such fluctuating forces may cause structural vibrations, acoustic noise and resonance, which in some cases can trigger structure failure or enhance mixing in the wake (Williamson, 1996). Therefore, it is very important to appropriately control vortex shedding in practical engineering environments.

Uniform flow past a circular cylinder has been accepted as a building-block problem for understanding the vortex dynamics in the wake behind a bluff body and, thus, a considerable number of studies on the uniform flow have been performed so far [refer to Williamson (1996) and Zdravkovich (1997) for more detailed reviews]. In most bluff-body flows of engineering interest, however, the free-stream is not uniform, but *sheared*. As evidently observed, air and tidal currents have nonzero velocity gradients in space and, thus, can be regarded as sheared. Such examples involve buildings and transport vehicles on the ground and pipelines under the sea. Nevertheless, shear flow or nonuniform flow over a circular cylinder has been investigated less extensively than uniform flow. Therefore, more systematic study on the shear flow is required for further improved understanding of engineering bluff-body flows. For such a study, the

*Tel.: +82 51 200 7636; fax: +82 51 200 7656.
E-mail address: kangsm@dau.ac.kr.

0889-9746/$ - see front matter
doi:10.1016/j.jfluidstructs.2006.02.003

shear flow can be assumed, as a first approximation, to have a constant lateral velocity gradient in the free-stream, that is a linear velocity profile across the cylinder diameter.

As depicted in Fig. 1(a), the free-stream with a linear velocity profile, $U = U_c + Gy$, passes over a circular cylinder with a diameter, D, where U_c and G are, respectively, the streamwise velocity at the center-line ($y = 0$) and the lateral velocity gradient ($G = \mathrm{d}U/\mathrm{d}y$). Therefore, the flow is governed by the three nondimensional flow parameters: one is the Reynolds number, $\mathrm{Re} = U_c D/\nu$, and another is the nondimensional velocity gradient or shear rate, $K = GD/U_c$, where ν is the kinematic viscosity; the third is introduced in what follows. In most of the previous experimental studies on the uniform-shear flow (Kiya et al., 1980; Kwon et al., 1992; Hayashi et al., 1993; Sumner and Akosile, 2003), the lateral width, W, of the flow domain was restricted such that the streamwise velocity in the free-stream was constantly positive ($U > 0$), that is the free-stream could not flow in the reverse direction due to the imposed shear rate. Accordingly, the blockage effect should be inevitably involved in the previous experimental results (Sumner and Akosile, 2003). Likewise, the present study will also restrict the lateral width to a finite extent, implying that the blockage ratio, defined as $B = D/W$, is the third flow parameter governing the uniform-shear flow.

So far, quite a few studies have been performed on uniform-shear flow over a circular cylinder and the typical ones are listed, along with the adopted flow conditions, in Table 1. They have mainly investigated the effects of Reynolds number and shear rate on the vortex-shedding frequency, the magnitude and direction of the mean lift, the magnitude of the mean drag, and so on in the uniform-shear flow. Despite many achievements to date, some controversial issues have to be further resolved for improved understanding of the bluff-body flow. As Lei et al. (2000) and Sumner and

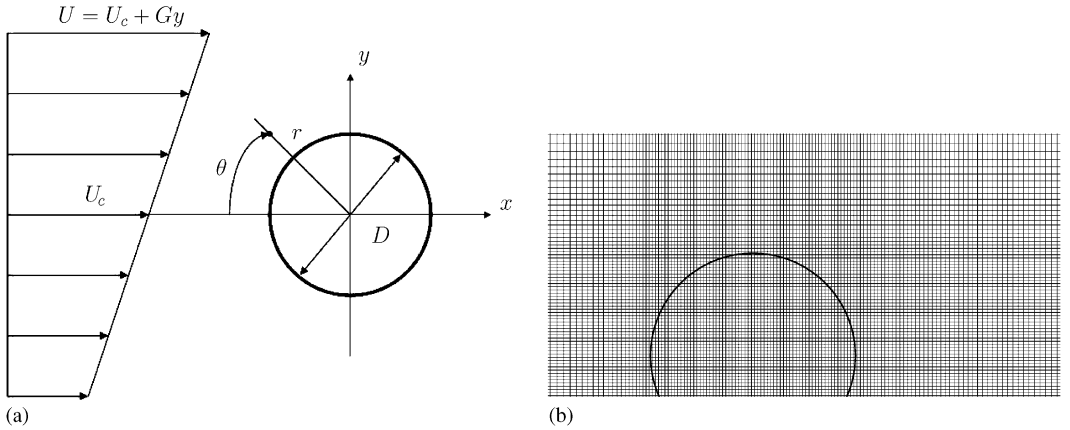

Fig. 1. (a) Schematic diagram of uniform-shear flow over a circular cylinder and (b) the computational mesh around the cylinder for the case of $B = 0.1$ ($M \times N = 513 \times 193$).

Table 1
Flow conditions used in previous studies

Researchers	Flow conditions			Method
	Re	K	B (%)	
Jordan and Fromm (1972)	400	See caption	≈ 0	CFD
Tamura et al. (1980)	40, 80	0−0.4	≈ 0	CFD
Kiya et al. (1980)	35−1500	0−0.25	2.7−17	EM
Yoshino and Hayashi (1984)	80	0−0.4	≈ 0	CFD
Kwon et al. (1992)	600−1600	0−0.25	6.7−16	EM
Hayashi et al. (1993)	6×10^4	0−0.045, 0.15	6.7	EM
Wu and Chen (2000)	−	0−2.67	≈ 0	CFD
Lei et al. (2000)	80−1000	0−0.25	12.5	CFD
Sumner and Akosile (2003)	$4-9 \times 10^4$	0.02−0.07	1.8−2.7	EM

CFD = computational fluid dynamics, EM = experimental measurement. Jordan and Fromm (1972) used the time-averaged flow of a turbulent jet for the uniform-shear flow case.

Akosile (2003) also pointed out, a few apparent discrepancies among previous studies on the uniform-shear flow remain unresolved yet. It is implied that more investigations on the uniform-shear flow are necessary, which motivates the present study. Representative controversial issues among previous studies are enumerated as follows.

Kiya et al. (1980) and Kwon et al. (1992) claimed that the vortex-shedding frequency, f, or the Strouhal number, $\mathrm{St} = fD/U_c$, increased with increasing shear rate mainly for large shear rates. Lei et al. (2000) and Sumner and Akosile (2003), on the other hand, claimed that the shedding frequency remained nearly constant or slightly decreased. Moreover, Kiya et al. (1980) reported that vortex shedding completely disappeared for sufficiently large shear rates ($K \geqslant 0.06$) in the range of $43 < \mathrm{Re} < 220$ considered in their experimental study. In the numerical study of Lei et al. (2000), however, the vortex shedding still occurred even under flow conditions similar to those of Kiya et al. ($\mathrm{Re} > 80$). The direction of the mean lift force has also to be addressed with regard to the conflicting issues among previous studies. Jordan and Fromm (1972), Hayashi et al. (1993), Lei et al. (2000) and Sumner and Akosile (2003) claimed that the mean lift was exerted from the side of the higher free-steam velocity to that of the lower one, whereas Tamura et al. (1980) and Yoshino and Hayashi (1984) asserted that it was in the opposite direction. In addition, Wu and Chen (2000) argued that the mean-lift direction should vary depending on the magnitude of shear rate.

Fig. 2 shows the variations of the mean drag coefficient, $\overline{C}_D$, the r.m.s. (root mean square) value of lift-coefficient fluctuations, C'_L, and the vortex-shedding frequency Strouhal number, St, with the blockage ratio for uniform flow over a circular cylinder ($K = 0$) at $\mathrm{Re} = 100$, together with the results of Park et al. (1998) and Norberg (2001) ($B \approx 0$). Details of the numerical method will be explained in the next section. Results show that the flow statistics, $\overline{C}_D$, C'_L and St, remain nearly constant for small blockage ratios, which are comparable to those of Park et al. (1998) and Norberg (2001). However, they all sharply deviate from their respective corresponding values achieved at $B \approx 0$ with increasing blockage ratio in the range of $B \gtrsim 0.05$. Very similar results can also be found in Zdravkovich (1997) and Chakraborty et al. (2004). Such a series of results indicate that the blockage ratio may exert a significant effect not only on the uniform flow, but also on the uniform-shear flow.

In previous experimental studies (Kiya et al., 1980; Kwon et al., 1992), the Reynolds number ($\mathrm{Re} = U_c D/\nu$) and shear rate ($K = GD/U_c$) were adjusted, mainly by changing the cylinder diameter, D, rather than the free-stream velocity profile, U_c and G, while restricting the lateral width of the flow domain due to facility limitations. This led to a serious problem that the blockage ratio ($B = D/W$) could not be kept constant when the cylinder diameter was changed. Sumner and Akosile (2003) argued that, in such a case, the blockage ratio should affect the uniform-shear flow to a considerable degree. Unlike the previous experimental studies (Kiya et al., 1980; Kwon et al., 1992), they exerted efforts to have the change in the blockage ratio as small as possible; refer to Table 1. The blockage effect on the uniform-shear flow also has to be thoroughly investigated. In most previous studies, however, this has not been done. The present study will investigate the blockage effect on uniform-shear flow over a circular cylinder and then provide results necessary to elucidate plausible causes of apparent discrepancies among previous studies on the uniform-shear flow. The main advantage of a numerical simulation is that the shear rate can be varied independently of the Reynolds number and blockage ratio, which cannot easily be done (or is nearly impossible) in experiments.

The objectives of the present study are to numerically investigate the characteristics of two-dimensional laminar uniform-shear flow over a circular cylinder, and then to further examine the corresponding underlying mechanism. For the study, we will concentrate on scrutinizing the effects of Reynolds number, shear rate and blockage ratio on the uniform-shear flow. Numerical simulations using the immersed-boundary method developed by Kim et al. (2001) are

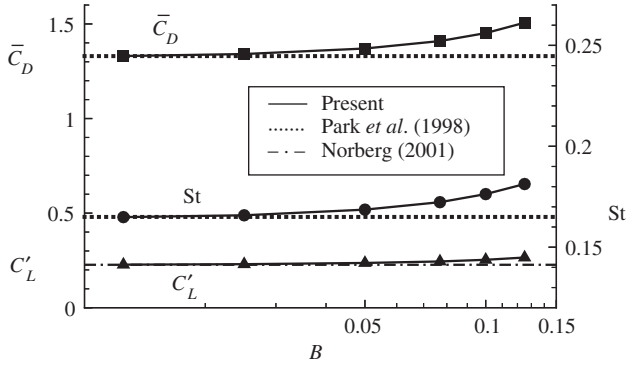

Fig. 2. Mean drag coefficient, root-mean-squared lift-coefficient fluctuation, and vortex-shedding frequency with respect to B for uniform flow over a circular cylinder ($K = 0$) at $\mathrm{Re} = 100$.

performed for simulating flows over or inside complex geometries. In the immersed-boundary method, both momentum forcing and mass source/sink are applied on the body surface or inside the body to satisfy the no-slip condition and continuity on or around the immersed boundary, leading to significant memory and CPU savings and easy grid generation compared to the unstructured grid method. In the present study, we will deal with the flow in the ranges of $50 \leqslant \mathrm{Re} \leqslant 160$, $0 \leqslant K \leqslant 0.2$, and $B = 0.1$ and 0.05 that is assumed to be two-dimensional and laminar.

2. Numerical method

Numerical simulations of two-dimensional unsteady incompressible flow with uniform planar shear over a circular cylinder are conducted using the immersed-boundary method. The appropriate governing equations can be written as

$$\frac{\partial u_i}{\partial t} + \frac{\partial (u_i u_j)}{\partial x_j} = -\frac{\partial p}{\partial x_i} + \frac{1}{\mathrm{Re}} \frac{\partial^2 u_i}{\partial x_j \partial x_j} + f_i, \tag{1}$$

$$\frac{\partial u_i}{\partial x_i} - q = 0. \tag{2}$$

Here, x_i are the Cartesian coordinates, u_i the corresponding velocity components, and p the pressure. All the variables are nondimensionalized by the cylinder diameter, D, and the streamwise velocity of the free-stream at the center-line ($y = 0$), U_c. For example, the velocity components are nondimensionalized by U_c, while the pressure by ρU_c^2. Notice that the notation sets (u, v) and (x, y) are used interchangeably with (u_1, u_2) and (x_1, x_2), respectively, in this paper. The discrete-time momentum forcing, f_i, is applied to satisfy the no-slip condition on the immersed boundary, whereas the mass source/sink, q, is to satisfy the mass conservation for the cell containing the immersed boundary. Therefore, f_i and q are defined, respectively, only at the faces and center of the cell on the immersed boundary or inside the body.

The governing equations, (1) and (2), are integrated in time using a second-order semi-implicit fractional-step method: a third-order Runge–Kutta method (RK3) for the convection terms and a second-order Crank-Nicolson method for the diffusion terms. In this method, a pseudo-pressure, ϕ, is introduced to correct the velocity field so that the continuity equation is satisfied at each computational time step. In space, on the other hand, the governing equations are resolved with a finite-volume approach on a staggered mesh. Here, the Cartesian (x, y) coordinate system is adopted as a basis for the application of the immersed-boundary method. In addition, a second-order linear or bilinear interpolation scheme is applied to satisfy the no-slip condition on the immersed boundary. More details associated with the immersed-boundary method are described in Kim et al. (2001).

Since, in the present study, the reverse-direction flow is not allowed in the free-stream, the lateral width of the flow domain and, thus, the maximum applicable shear rate are determined depending on the adopted blockage ratio. The present computational domain extends to $|x| \leqslant 40$ and $|y| \leqslant 1/(2B)$ and the circular cylinder is located with its center at $(0, 0)$. In addition, the shear rate to be applied, depending on the blockage ratio, is $K \leqslant 2B$; for example $K \leqslant 0.2$ for $B = 0.1$ and $K \leqslant 0.1$ for $B = 0.05$. A Dirichlet boundary condition of the uniform-shear steady flow, $u = 1 + Ky$ and $v = 0$, is used at the inflow ($x = -40$), and a convective outflow condition, $\partial u_i/\partial t + c\partial u_i/\partial x = 0$, is used at the outflow ($x = 40$) where c is the space-averaged streamwise exit velocity. The no-slip condition, $u = 0$ and $v = 0$, is imposed on the immersed boundary or the cylinder surface expressed with $x^2 + y^2 = 0.5^2$. At the far-field boundaries [$y = \pm 1/(2B)$], on the other hand, two kinds of boundary conditions are attempted for checking their suitability to the present study: one is a constant-vorticity condition, $\omega = -K$ (or $\partial u/\partial y = K$) and $v = 0$, and the other is a constant-velocity condition, $u = 1 \pm K/(2B)$ and $v = 0$. It is found that the two boundary conditions do not lead to any significant difference in the computational results. Therefore, we will present only the results achieved from the former condition in the present paper. In addition, the Neumann condition of $\partial\phi/\partial x_n = 0$ (x_n is the normal direction) is applied at the boundary to solve the Poisson equation for the pseudo-pressure, ϕ.

For more efficient simulations, the computational domain is spatially resolved such that a dense clustering of grid points is applied near the cylinder, especially in the wake zone, while away from the cylinder a coarser grid is used. In the present study, a uniform distribution of 64×64 grid points is used within the cylinder diameter, whereas the tangential-hyperbolic grid distribution is in the outer region. As the lateral width of the flow domain changes, the number of total grid points in the y direction is properly adjusted such that the resolution close to the cylinder is preserved. For example, the spatial resolutions are $M \times N = 513 \times 193$ for $B = 0.1$ [see Fig. 1(b)] and 513×225 for $B = 0.05$.

A computational time step of $\Delta t = 0.008 - 0.01$ is used for time advancement in all the simulations performed in the present study. All the simulations are continued until the flow reaches a fully developed state, where all the flow

Table 2
Validation of the numerical method: parametric study for uniform-shear flow over a circular cylinder at Re = 100 and $K = 0.2$ in the case of $B = 0.1$

Re	K	$M \times N$	Δx_c (Δy_c)	Δt	St	$\overline{C}_L$	$\overline{C}_D$	C'_L	C'_D
100	0.2	513×193	1/64	0.0100	0.1696	−0.1732	1.3943	0.2699	0.0254
		705×289	1/96	0.0064	0.1697	−0.1721	1.3941	0.2702	0.0254
					(0.06)	(0.64)	(0.01)	(0.11)	(0.00)

Here, in parentheses are the relative errors (%) with respect to the result from $M \times N = 513 \times 193$ and $\Delta t = 0.01$. Δx_c and Δy_c denote the magnitudes of grid spacings inside and around the cylinder.

Table 3
Validation of the numerical method: comparison study for unconfined uniform flow over a circular cylinder ($K = 0$) at Re = 100 ($M \times N = 513 \times 193$ and $\Delta t = 0.01$)

	$\overline{C}_D$	C'_L	St	Remarks
Present	1.33	0.228	0.165	$B = 0.0125$
Williamson (1996)			0.164	
Park et al. (1998)	1.33		0.165	
Norberg (2001)		0.227	0.165	
Stojković et al. (2002)	1.34		0.165	

characteristics are analyzed. Since the fully developed flow is independent of initial conditions, all the simulations may be started with arbitrary initial conditions.

To confirm the spatial and temporal convergence, parametric studies for the uniform-shear flow at Re = 100 and $K = 0.2$ have been performed and the typical results are presented in Table 2. Here, $\overline{C}_L$ and $\overline{C}_D$ are the mean (time-averaged) lift and drag coefficients [i.e. $\overline{C}_L = (\int_t^{t+T} C_L \, dt)/T$, where T is a period in the fully developed state], while C'_L and C'_D are the r.m.s values of the lift- and drag-coefficient fluctuations [i.e. $C'_L = \{\int_t^{t+T} (C_L - \overline{C}_L)^2 \, dt)/T\}^{1/2}$]. The relative errors in the table show that the computational results obtained with the chosen parameter values are well converged with respect to the spatial and temporal resolutions. Subsequently, the same numerical simulations have also been performed on uniform flow over a circular cylinder ($K = 0$) for a very low blockage ratio ($B = 0.0125$), and their typical results are compared with the previously published data in Table 3 and Fig. 3. The comparisons show that the present results are in excellent agreement with the existing ones, certainly validating the present immersed-boundary method.

3. Results

After verifying the numerical method, we have conducted numerical simulations by systematically varying the Reynolds number, shear rate and blockage ratio in the fairly wide ranges of $50 \leqslant \mathrm{Re} \leqslant 160$, $0 \leqslant K \leqslant 0.2$, and $B = 0.1$ and 0.05.

3.1. Flow statistics

3.1.1. Vortex-shedding frequency

Fig. 4 shows the variations of the vortex-shedding frequency with the Reynolds number, shear rate and blockage ratio in uniform-shear flow over a circular cylinder. According to Fig. 4(a), with increasing Reynolds number, the shedding frequency markedly increases all over the ranges of the shear rate and blockage ratio considered in the present study. On the other hand, the shedding frequency remains nearly constant or slightly decreases with increasing shear rate, while it increases with increasing blockage ratio. In the laminar regime ($\mathrm{Re} < 200$), the effect of Reynolds number

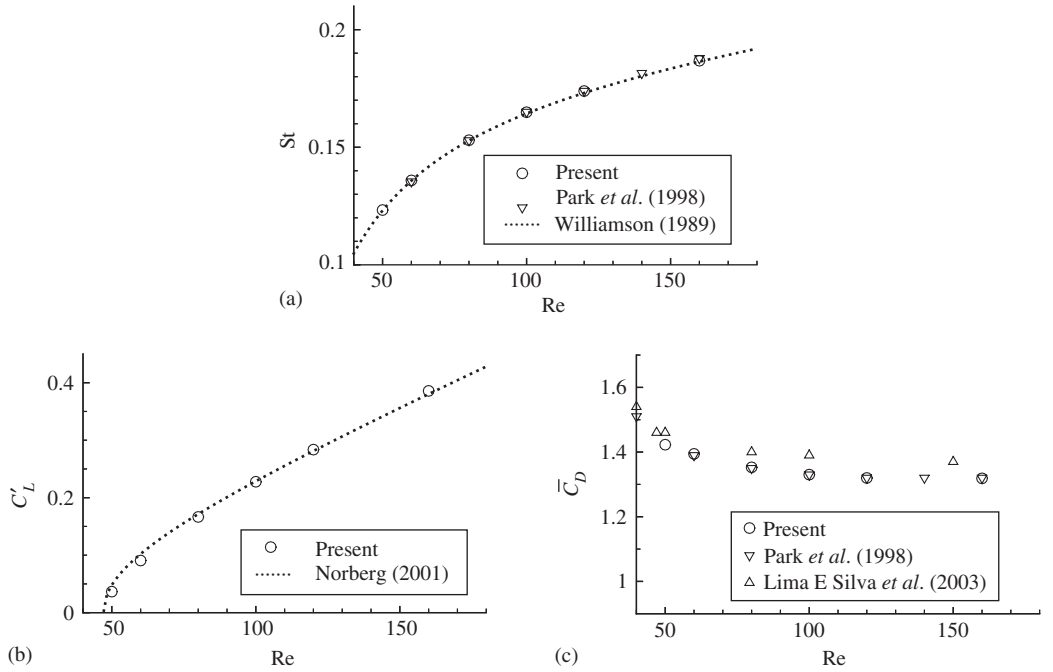

Fig. 3. Comparison of the present results ($K = 0$ and $B = 0.0125$) with the previously published data: (a) St, (b) C'_L, and (c) $\overline{C}_D$. Data for (a) has been taken from Williamson (1989) , (b) from Norberg (2001) and (c) from Lima E. Silva et al. (2003).

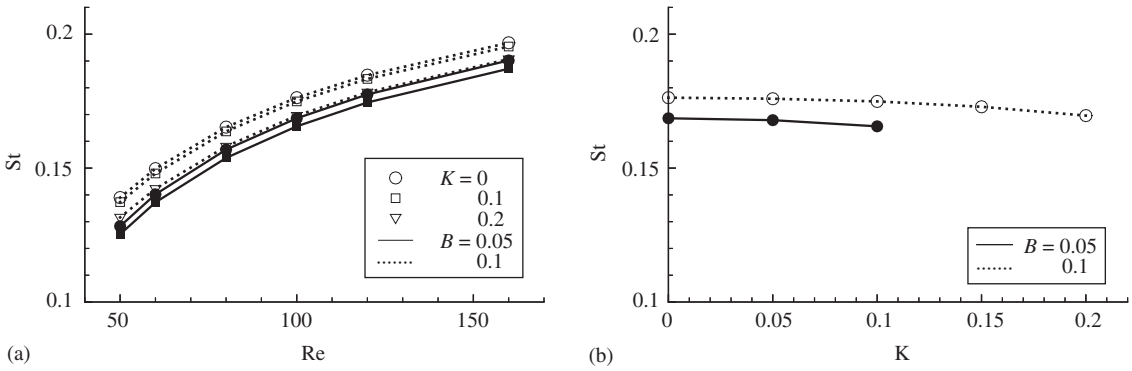

Fig. 4. Vortex-shedding frequencies with respect to Re, K and B: (a) St versus Re, and (b) St versus K (at Re = 100).

on the vortex-shedding frequency is overall very strong compared with those of the shear rate and blockage ratio. To more closely reveal the shear effect, the variation of the shedding frequency with the shear rate is presented in Fig. 4(b) for the uniform-shear flow at Re = 100. With increasing shear rate, the shedding frequency remains nearly constant for low shear rates and then slightly decreases for $K \gtrsim 0.1$. Such correlation between the shedding frequency and shear rate agrees well with those of Lei et al. (2000) and Sumner and Akosile (2003), but substantially differs from those of Kiya et al. (1980) and Kwon et al. (1992).

Kiya et al. (1980) and Kwon et al. (1992) varied the cylinder diameter, while fixing the velocity profile in the free-stream (U_c and G), to adjust the Reynolds number ($\mathrm{Re} = U_c D/\nu$) and shear rate ($K = GD/U_c$) in their experimental studies on the uniform-shear flow. Consequently, they could not keep the blockage ratio constant while the flow parameters were varied. For example, the blockage ratios were in the ranges of $B = 2.7-17(\%)$ and $6.7-16(\%)$ in the studies of Kiya et al. (1980) and Kwon et al. (1992), respectively, and thus the variance widths were excessively large; see Table 1. According to Fig. 4(b), the difference in the vortex-shedding frequency between two blockage ratios of $B = 5(\%)$ and $10(\%)$ is larger than that between two shear rates of $K = 0$ and 0.2 for the uniform-shear flow at

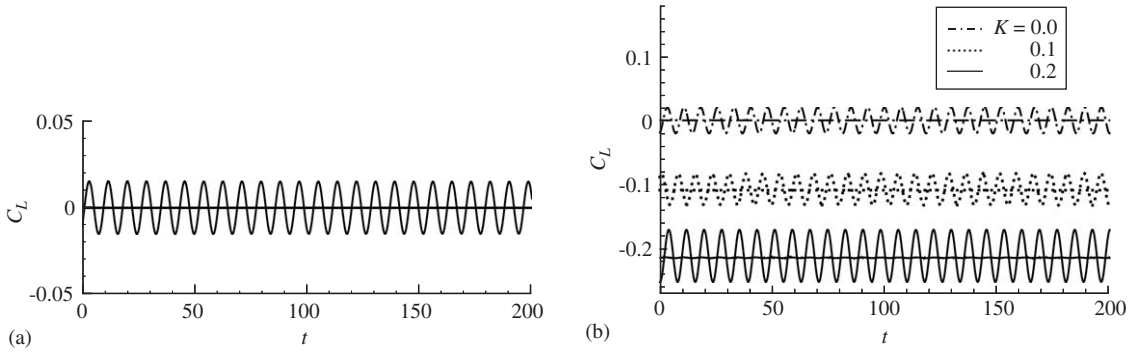

Fig. 5. Time evolutions of the lift coefficient: (a) for the flow at $\mathrm{Re} = 46$ (steady) and 47 (time-periodic) in the case of $B = 0.0125$ and (b) for the flow at $\mathrm{Re} = 45$ (steady) and 47 (time-periodic) with respect to K in the case of $B = 0.1$.

$\mathrm{Re} = 100$, which obviously indicates the significance of the blockage effect in identifying exactly the correlation between the shedding frequency and shear rate. It is, therefore, implied that the blockage effect may provide a meaningful clue for plausible causes of apparent discrepancies among previous studies on the flow. Recently, Sumner and Akosile (2003) made an effort to keep the blockage ratio as constant as possible in their experimental study [$B = 1.8-2.7(\%)$], to avoid a probably erroneous interpretation due to its large variance. Even in the uniform-shear flow at very high Reynolds numbers ($\mathrm{Re} = 4-9 \times 10^4$), they found that the shedding frequency slightly decreased with increasing shear rate, which is in good agreement with the present study.

Kiya et al. (1980) reported that vortex shedding completely disappeared for sufficiently large shear rates in the uniform-shear flow in the range of $43 < \mathrm{Re} < 220$ considered in their experiment. Then, they claimed that the critical Reynolds number, Re_c, above which vortex shedding occurred, increased linearly in proportion to the shear rate for $K \geqslant 0.06$. On the contrary, such a phenomenon was not observed in the numerical study of Lei et al. (2000) which was performed under similar flow conditions ($\mathrm{Re} > 80$). It is generally known that, in the uniform flow ($K = 0$ and $B \approx 0$), vortex shedding occurs when the Reynolds number exceeds approximately 47 ($\mathrm{Re} \geqslant \mathrm{Re}_c \approx 47$) (Park et al., 1998; Fey et al., 1998; Norberg, 2001). Fig. 5(a) confirms that the observation can also be exactly reproduced for the uniform flow ($K = 0$) at a very small blockage ratio ($B = 0.0125$) in the present study. To see the variation of the critical Reynolds number with the shear rate, numerical simulations for the uniform-shear flow at $\mathrm{Re} = 45$ and 47 in the case of $B = 0.1$ have been performed and typical results are presented in Fig. 5(b). In all the simulations performed, vortex shedding still occurs at $\mathrm{Re} = 47$ but completely disappears at $\mathrm{Re} = 45$, implying that the critical Reynolds number ($\mathrm{Re}_c \approx 46-47$) hardly relates to the shear rate and blockage ratio for the whole ranges of K and B considered. It is suggested that additional three-dimensional simulations should be performed to figure out plausible causes of the discrepancy between the present study and that of Kiya et al. (1980) on the uniform-shear flow.

3.1.2. *Lift and drag coefficients*

In uniform-shear flow over a circular cylinder, the direction of the lift force is not only of great engineering importance, but also one of the most controversial issues among previous studies. Fig. 6 shows the variations of the mean (time-averaged) lift coefficient, $\overline{C}_L$, and the r.m.s. value of lift-coefficient fluctuations, C'_L, with the Reynolds number, shear rate and blockage ratio. In the case of a positive shear rate ($K > 0$), the mean lift coefficient is negative ($\overline{C}_L < 0$) all over the ranges of the Reynolds number and blockage ratio considered in the present study, indicating that the mean lift is exerted from the side of the higher free-stream velocity to that of the lower one. Despite the difference in the Reynolds number, the present results agree well with those of Jordan and Fromm (1972), Hayashi et al. (1993), Lei et al. (2000), and Sumner and Akosile (2003), but substantially differ from those of Tamura et al. (1980), Yoshino and Hayashi (1984), and Wu and Chen (2000). Such discrepancies were also pointed out by Lei et al. (2000) and Sumner and Akosile (2003), but a plausible reason has not yet been forthcoming.

According to Fig. 6, the magnitude of the mean lift, $-\overline{C}_L$ or $|\overline{C}_L|$, slightly decreases with increasing either Reynolds number or blockage ratio, but greatly increases linearly in proportion to the shear rate. To quantify the linear relation between the mean lift and shear rate, the least-squares fit for the uniform-shear flow at $\mathrm{Re} = 100$ provides $\overline{C}_L \sim -0.96K$ and $-0.86K$ for $B = 0.05$ and 0.1, respectively. On the other hand, the lift fluctuation largely increases with increasing Reynolds number, but slightly increases or remains nearly constant with increasing either shear rate or blockage ratio. In addition, the lift fluctuation is very low without regard to the shear rate and blockage ratio at $\mathrm{Re} = 50$, near the critical Reynolds number ($\mathrm{Re}_c \approx 46-47$).

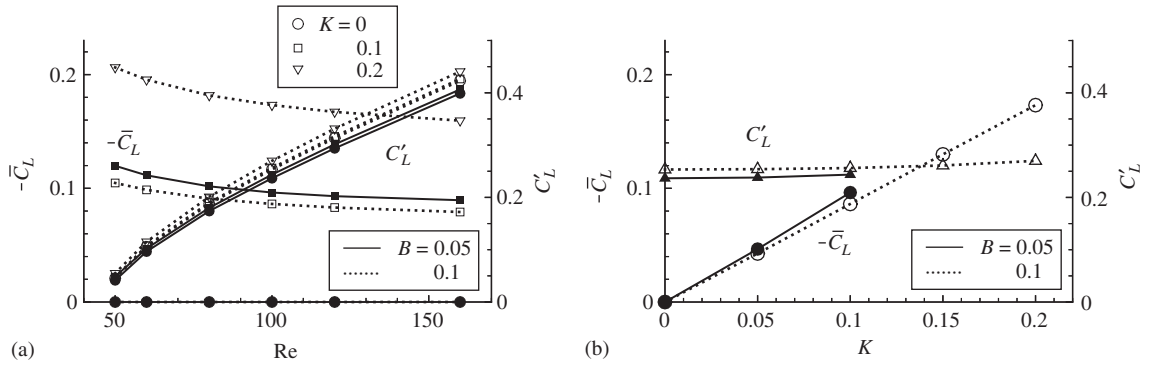

Fig. 6. Mean lift coefficients and r.m.s. values of lift-coefficient fluctuations with respect to Re, K and B: (a) $-\overline{C}_L$ and C'_L versus Re and (b) $-\overline{C}_L$ and C'_L versus K (at Re = 100).

Meanwhile, it is remarkable to compare the present result on the mean lift with that for the cylindrical bubble whose outer surface does not sustain any shear stress. In general, the cylindrical-bubble flow can be reasonably analyzed by considering inviscid flow past a circular cylinder with a uniform lateral velocity-gradient. For that study, Tsien (1943) quantified the shear effect using a stream function, ψ, derived from the potential theory as follows [see Zdravkovich (1997) for more details]:

$$\psi = \left(r - \frac{1}{4r}\right)\sin\theta + \frac{K}{2}\left(r^2\sin^2\theta + \frac{1}{32r^2}\cos 2\theta\right) \tag{3}$$

satisfying

$$\frac{1}{r}\frac{\partial}{\partial r}\left(r\frac{\partial\psi}{\partial r}\right) + \frac{1}{r^2}\frac{\partial\psi}{\partial\theta^2} = K, \tag{4}$$

$$\left.\frac{1}{r}\frac{\partial\psi}{\partial\theta}\right|_{r=1/2} = 0. \tag{5}$$

Here, Eq. (4) implies a constant background vorticity, $\omega = -K$, throughout the flow field, while Eq. (5) denotes a zero normal velocity on the cylinder surface. Computing the velocity profile and then the pressure distribution on the cylinder surface from Eq. (3), through potential theory, yields the following lift coefficient:

$$C_L = \pi K. \tag{6}$$

Similarly, the position of the stagnation point, θ_o, can also be computed as follows:

$$\sin\theta_o = \frac{-1 + [1 + (K/2)^2]^{1/2}}{K}. \tag{7}$$

For a positive shear rate ($K > 0$), Eq. (6) denotes a positive lift coefficient ($C_L > 0$), while Eq. (7) indicates the existence of the stagnation points on the upper surface of the cylinder. It is, therefore, implied that, even if the stagnation points exist on the upper cylinder surface, the lift force acts from the side of the lower free-stream velocity to that of the higher one ($+y$ direction). In addition, its magnitude increases linearly in proportion to the shear rate.

The Tsien (1943) study tells that the lift direction for the solid cylinder may be totally different from that for the cylindrical bubble. Such similar discussions can work for the case of a sphere: refer to Legendre and Magnaudet (1998), Kurose and Komori (1999), and Bagchi and Balachandar (2002). These studies showed that the lift direction was positive for the spherical bubble. On the other hand, for the solid sphere, the lift direction was negative at moderate to high Reynolds numbers, whereas it was positive at moderate to low Reynolds numbers. From the results, it can be concluded that the negative lift force in uniform-shear flow over a circular cylinder is probably due to the no-slip condition on the surface.

The variations of the mean drag coefficient, $\overline{C}_D$, and the r.m.s. value of drag-coefficient fluctuations, C'_D, with the Reynolds number, shear rate and blockage ratio are shown in Fig. 7. The mean drag decreases with increasing Reynolds number and simultaneously the decline rate also decreases. In the case of shear rate, the mean drag remains nearly constant for low shear rates, and then slightly decreases with increasing shear rate for $K \gtrsim 0.1$. The variation behavior agrees well with those of previous studies (Kwon et al., 1992; Hayashi et al., 1993; Lei et al., 2000; Sumner and Akosile,

2003). In addition, with increasing blockage ratio, the mean drag greatly increases regardless of the Reynolds number and shear rate, which implies that the blockage effect plays an important role in the characteristics of uniform-shear flow over a circular cylinder. Nevertheless, the blockage effect has been treated as trivial in most of the previous studies on uniform-shear flow. On the other hand, the drag fluctuation that is negligibly small near the critical Reynolds number increases approximately linearly in proportion to $(\mathrm{Re} - \mathrm{Re}_c)$. In addition, the drag fluctuation also rises with increasing shear rate. However, the blockage effect on the drag fluctuation is not so large.

The behavior of the lift and drag forces presented in Figs. 6 and 7 can be represented more clearly in the form of phase diagrams by plotting C_D as a function of C_L. The phase diagrams according to the shear rate and blockage ratio for the uniform-shear flow at $\mathrm{Re} = 100$ are shown in Fig. 8. All the phase diagrams have a closed shape of the infinity symbol (∞), which indicates that all the flows become completely time-periodic in the fully developed state. As evident

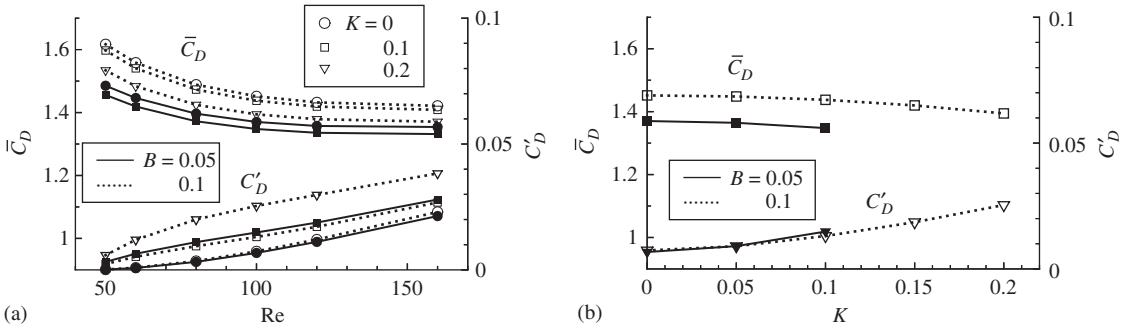

Fig. 7. Mean drag coefficients and r.m.s. values of drag-coefficient fluctuations with respect to Re, K and B: (a) $\overline{C}_D$ and C'_D versus Re and (b) $\overline{C}_D$ and C'_D versus K (at $\mathrm{Re} = 100$).

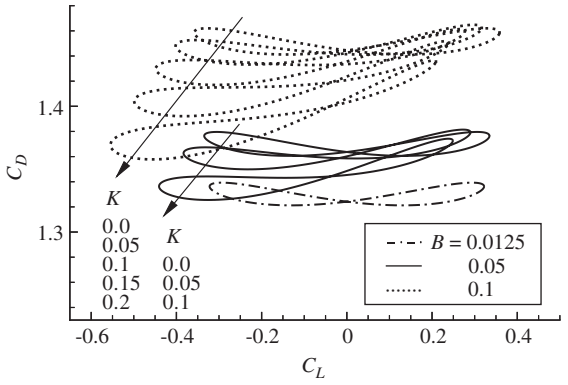

Fig. 8. Phase diagrams of C_D versus C_L with respect to K and B for the uniform-shear flow at $\mathrm{Re} = 100$.

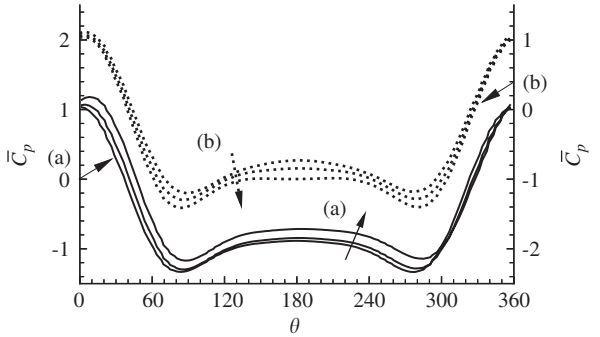

Fig. 9. Mean pressure coefficients around the cylinder surface plotted according to Re and K for the uniform-shear flow in the case of $B = 0.1$: (a) $K = 0$, 0.1 and 0.2 for $\mathrm{Re} = 100$ (left axis), and (b) $\mathrm{Re} = 60$, 100 and 160 for $K = 0.1$ (right axis).

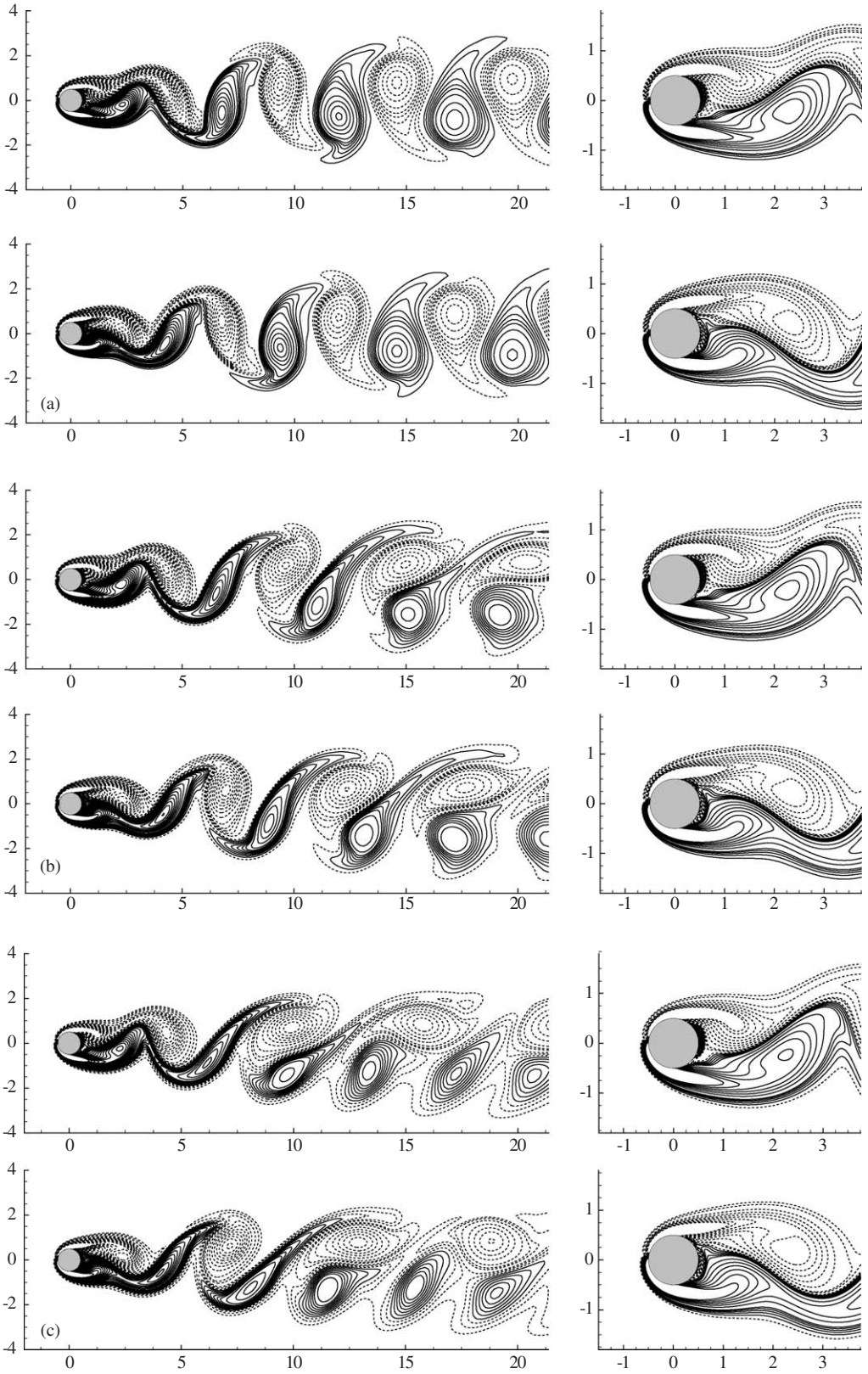
(a)
(b)
(c)

in the figure, the position of a phase diagram denotes the mean lift and drag and the size denotes the corresponding fluctuation amplitudes. The phase diagrams shown in Fig. 8 confirm again the significant effects of shear rate and blockage ratio on the uniform-shear flow. In some cases, especially, the position of the closed curve depends more strongly on the blockage ratio than on the shear rate, implying that the blockage ratio may significantly alter the flow characteristics. It is also shown that the blockage ratio affects more strongly the drag force than the lift. On the other hand, the phase diagram hardly varies for $C_L > 0$ even for the change of shear rate. However, the phase diagram greatly varies for $C_L < 0$, thus overall decreasing the mean drag force or the minimum lift force. These observations are in exact agreement with those depicted in Figs. 6 and 7.

3.1.3. Mean pressure coefficient

It is generally known that, in flow over a bluff body such as a circular cylinder and a sphere, the effect of friction on the lift force is negligibly small compared to the pressure (Park et al., 1998; Fey et al., 1998; Mittal and Kumar, 2003). Therefore, to further understand the effects of Reynolds number and shear rate on the lift force, it is essential to know exactly the pressure distribution around the cylinder surface. Fig. 9 shows the mean (time-averaged) pressure coefficient, $\overline{C}_p$, according to the Reynolds number and shear rate. The mean pressure coefficient is defined as $\overline{C}_p(\theta) = 2[\overline{p}(\theta) - p_c]/\rho U_c^2$, where p_c is the pressure corresponding to the free-stream velocity, U_c, at the center-line ($y = 0$) far away from the cylinder and $\overline{p}(\theta)$ is the mean pressure at θ. Note that the range of $\theta = 0{-}180^\circ$ corresponds to the side of the higher free-stream velocity. As expected, the mean pressure for the zero-shear flow (at $K = 0$) is symmetric about $\theta = 0{-}180^\circ$ (front and base points), leading to a zero mean lift. As the shear rate increases, the flow becomes asymmetric. That is, the stagnation point involving the maximum pressure on the cylinder surface moves to the higher-velocity side. Simultaneously, the pressure hardly changes in the range of $\theta \approx 300{-}360^\circ$, whereas, out of the range, it greatly increases [see Fig. 9(a)]. A simple analysis of force balance indicates that the mean lift force acts from the side of the higher free-stream velocity to that of the lower one, and the magnitude greatly increases with increasing shear rate. On the other hand, as the Reynolds number increases, the pressure greatly decreases in the range of $\theta \approx 30{-}300^\circ$, whereas, out of the range, it slightly varies [see Fig. 9(b)]. Therefore, the mean lift force decreases in magnitude with increasing Reynolds number. These observations again confirm the results shown in Fig. 6.

3.2. Wake dynamics

Instantaneous flow fields have been investigated to further understand vortex shedding in uniform-shear flow over a circular cylinder and its corresponding underlying mechanism. Results show that, although the flow statistics depend significantly on the blockage ratio as shown in Figs. 4, 6 and 7, the appearance of the instantaneous flow field does not change so markedly. In the present paper, therefore, only the results for the uniform-shear flow at $B = 0.1$ will be presented. Fig. 10 shows the variation of the instantaneous vorticity contours with the shear rate for the uniform-shear flow at $\mathrm{Re} = 100$. In the figure, the vorticity contours at two different times corresponding to the maximum and minimum lift forces in one complete period are presented for each shear rate. Note that the background vorticity in each case is $\omega = -K$ and, thus, negative.

In the case of no shear ($K = 0$), vortices of positive and negative signs are alternately shed from the cylinder, and consequently move downstream. Thus, the flow becomes symmetric about the center-line ($y = 0$) in the sense of time-averaging. In the case of nonzero shear ($K > 0$), on the other hand, vortex shedding also occurs. Overall, with a negative background vorticity, the vortices of positive sign are weakened whereas those of negative sign are strengthened. At the same time, in the near wake behind the circular cylinder, the positive-signed vortices become more elongated, whereas the negative-signed ones become more round. The scenario for such vortex shapes can be explained as follows. Immediately after each negative-signed vortex is shed on the upper side ($+y$ direction), the downstream end of the vortex moves toward the lower side, that is toward the side of the lower free-stream velocity. Afterwards, the downstream end flows downstream more slowly than the upstream end due to the difference in the free-stream velocity and, thus, the vortex becomes of a round shape. Moreover, it is seen that the round shape becomes more conspicuous with increasing shear rate. For each positive-signed vortex shed from the lower side, on the contrary, the downstream end moves toward the side of the higher free-stream velocity. Therefore, the downstream end moves downstream faster than the upstream one, so that the vortex becomes elongated.

Fig. 10. Instantaneous vorticity contours at two times of the maximum (upper) and minimum (lower) lift forces in one complete period with respect to K for the uniform-shear flow at $\mathrm{Re} = 100$ and $B = 0.1$: $K =$ (a) 0.0, (b) 0.1, and (c) 0.2. Note that the background vorticity corresponds to $-K$ in each case. Contour levels on the left side (wider plots) are from -0.3 to 0.3 in increments of 0.05 and ± 0.4 to ± 3 in increments of 0.2, whereas those on the right side (closer plots) are from -0.3 to 0.3 in increments of 0.1 and ± 0.4 to ± 3 in increments of 0.4. Negative values are shown as dashed.

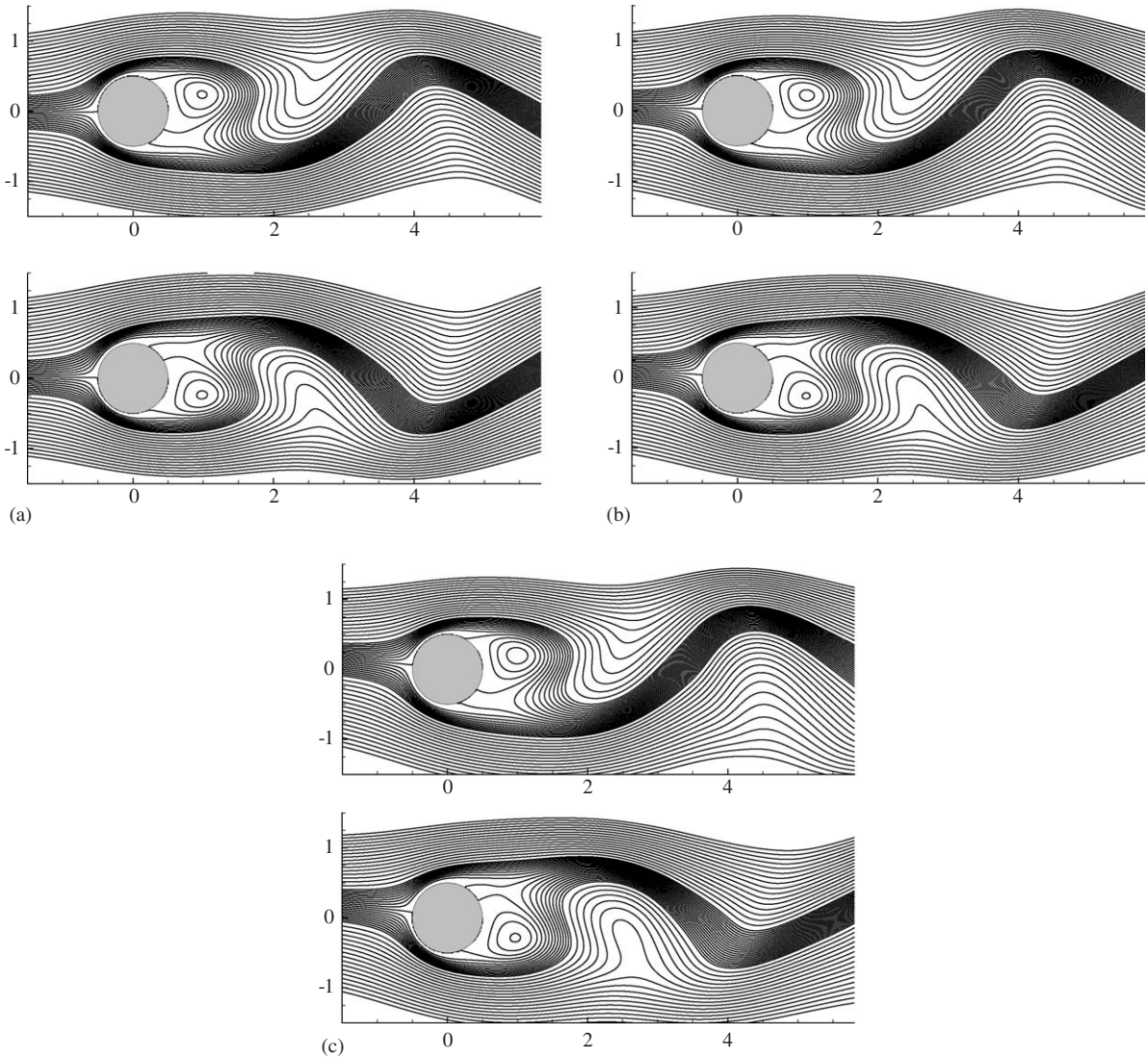

Fig. 11. Instantaneous streamlines at two times of the maximum (upper) and minimum (lower) lift forces in one complete period with respect to K for the uniform-shear flow at $\mathrm{Re} = 100$ and $B = 0.1$: $K =$ (a) 0.0, (b) 0.1, and (c) 0.2. Contour levels are from -0.2 to 0.2 in increments of 0.02 and ± 0.2 to ± 1 in increments of 0.05.

Due to the negative background vorticity, all the vortices are shifted in the clockwise direction as they travel downstream and, thus, the vortex street is inclined toward the side of the lower free-stream velocity. As is evident in Fig. 10(c), the positive- and negative-signed vortices are located, respectively, on the sides of the lower and higher free-stream velocities. With increasing shear rate, therefore, the distance between two subsequent negative-signed vortices increases, but for the positive-signed ones, the distance decreases.

Fig. 11 shows streamline contours corresponding to the vorticity contours presented in Fig. 10. It is known that the magnitude and direction in the mean lift force is determined mainly by the stagnation point. The figure indicates that, as the shear rate increases, the angle of attack of the free-stream increases and, thus, the stagnation point on the cylinder moves in the clockwise ($+\theta$) direction. According to the present numerical results, the stagnation points for $K = 0$, 0.1 and 0.2 move, respectively, as much as 0°, 3.7° and 9.2° (in the case of $B = 0.1$).

Fig. 12 shows the time evolution of the instantaneous vorticity field in one complete period for the uniform-shear flow at $\mathrm{Re} = 100$ and $K = 0.2$. This figure indicates the way the shed vortices are formed and convected downstream. It is seen that there are two alternate vortices over one period and the negative-signed vortex becomes strengthened and round-shaped due to the negative background vorticity ($\omega = -K < 0$). On the contrary, the positive-signed vortex

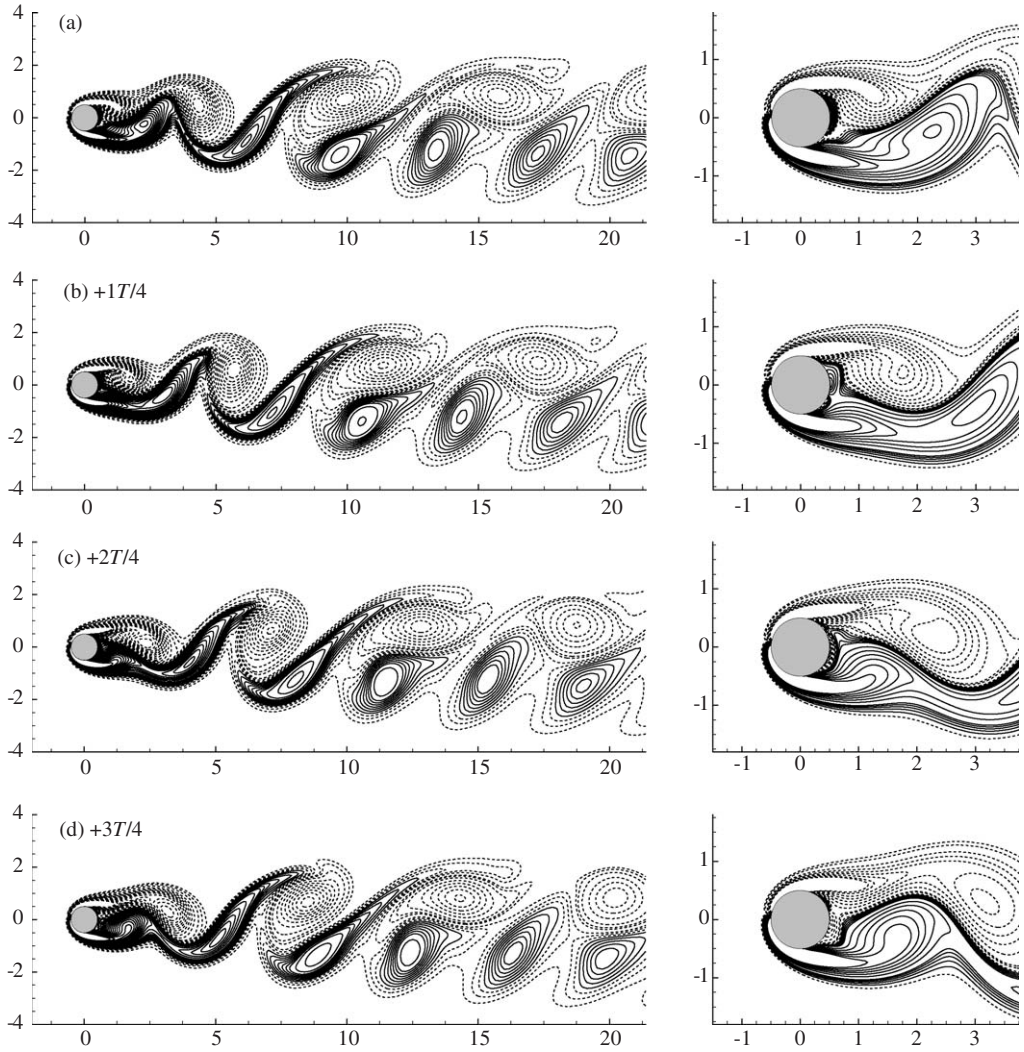

Fig. 12. Time evolution of the instantaneous vorticity contours for the uniform-shear flow at $\mathrm{Re} = 100$, $K = 0.2$ and $B = 0.1$: T denotes the period. Note that the background vorticity corresponds to $-K$. Contour levels on the left side (wider plots) are from -0.3 to 0.3 in increments of 0.05 and ± 0.4 to ± 3 in increments of 0.2, whereas those on the right side (closer plots) are from -0.3 to 0.3 in increments of 0.1 and ± 0.4 to ± 3 in increments of 0.4. Negative values are shown as dashed.

becomes weakened and more elongated. Far downstream, the round-shaped negative-signed vortex gradually becomes oval-shaped because of the difference in the free-stream velocity between the upper and lower sides about the vortex induced due to the negative background vorticity. On the contrary, the positive-signed vortex, originally of an elongated shape, becomes more and more elongated due to the negative background vorticity. Afterwards, the downstream end of the positive-signed vortex becomes very weak in strength and finally disappears, whereas the upstream end still remains oval-shaped.

4. Conclusions

In the present study, we have investigated numerically two-dimensional laminar flow over a circular cylinder with a uniform planar shear, where the free-stream velocity varies linearly across the cylinder, for the purpose of identifying the hydrodynamic force and wake dynamics and then describing the underlying mechanism. In this study, numerical simulations were performed, using the immersed boundary method developed by Kim et al. (2001), on the

uniform-shear flow in the ranges of $50 \leqslant \mathrm{Re} \leqslant 160$, $0 \leqslant K \leqslant 0.2$, and $B = 0.1$ and 0.05. Particularly, we have also examined the effect of lateral width in the flow domain, that is the blockage effect, to figure out plausible causes of apparent discrepancies among previous studies on the flow. Conclusions drawn in the present study can be summarized as follows.

(i) The vortex-shedding frequency significantly increased with increasing Reynolds number, while it remained nearly constant or slightly decreased with increasing shear rate. With increasing blockage ratio, on the other hand, the shedding frequency slightly increased all over the ranges of the Reynolds number and shear rate.

(ii) The mean lift was directed from the side of the higher free-stream velocity to the lower one. The magnitude of the mean lift slightly decreased with increasing Reynolds number or blockage ratio, but largely increased linearly in proportion to the shear rate. The lift fluctuation greatly increased with increasing Reynolds number, while it slightly increased or remained nearly constant with increasing either shear rate or blockage ratio.

(iii) The mean drag decreased with increasing Reynolds number, and remained nearly constant or slightly decreased with increasing shear rate. With increasing blockage ratio, on the other hand, the mean drag greatly increased. The drag fluctuations greatly increased with increasing Reynolds number or shear rate, but the blockage effect was not so significant.

(iv) There have been a few controversial issues among previous studies on uniform-shear flow over a circular cylinder. The present results showed that the blockage effect on the flow was comparable to the shear effect. It was implied that the blockage ratio might be one of the plausible causes of apparent discrepancies among previous studies.

(v) In the case of nonzero shear ($K > 0$), the background vorticity in the free-stream was negative. Therefore, the positive-signed vortices in the near-wake behind the circular cylinder became weakened and elongated, while the negative-signed ones became strengthened and round-shaped.

Acknowledgments

This work was supported by the NRL (National Research Laboratory) Program of the Ministry of Science and Technology, Korea.

References

Bagchi, P., Balachandar, S., 2002. Shear versus vortex-induced lift force on a rigid sphere at moderate Re. Journal of Fluid Mechanics 473, 379–388.

Chakraborty, J., Verma, N., Chhabra, R.P., 2004. Wall effects in flow past a circular cylinder in a plane channel: a numerical study. Chemical Engineering and Processing 43, 1529–1537.

Fey, U., Konig, M., Eckelmann, H., 1998. A new Strouhal–Reynolds-number relationship for the circular cylinder in the range $47 < \mathrm{Re} < 2 \times 10^5$. Physics of Fluids 10, 1547–1549.

Hayashi, T., Yoshino, F., Waka, R., 1993. The aerodynamic characteristics of a circular cylinder with tangential blowing in uniform shear flows. JSME International Journal Series B 36, 101–112.

Jordan, S.K., Fromm, J.E., 1972. Laminar flow past a circle in shear flow. Physics of Fluids 15, 972–976.

Kim, J., Kim, D., Choi, H., 2001. An immersed-boundary method finite-volume method for simulations of flow in complex geometries. Journal of Computational Physics 171, 132–150.

Kiya, M., Tamura, H., Arie, M., 1980. Vortex shedding from a circular cylinder in moderate-Reynolds-number shear flow. Journal of Fluid Mechanics 141, 721–735.

Kurose, R., Komori, S., 1999. Drag and lift on a rotating sphere in a linear shear flow. Journal of Fluid Mechanics 384, 183–206.

Kwon, T.S., Sung, H.J., Hyun, J.M., 1992. Experimental investigation of uniform-shear flow past a circular cylinder. ASME Journal of Fluids Engineering 114, 457–460.

Legendre, D., Magnaudet, D., 1998. The lift force on a spherical bubble in a viscous linear shear flow. Journal of Fluid Mechanics 368, 81–126.

Lei, C., Cheng, L., Kavanagh, K., 2000. A finite difference solution of the shear flow over a circular cylinder. Ocean Engineering 27, 271–290.

Lima E. Silva, A.L.F., Ailveira-Neto, A., Damasceno, J.J.R., 2003. Numerical simulation of two-dimensional flows over a circular cylinder using the immersed boundary method. Journal of Computational Physics 189, 351–370.

Mittal, S., Kumar, B., 2003. Flow past a rotating cylinder. Journal of Fluid Mechanics 476, 303–334.

Norberg, C., 2001. Flow around a circular cylinder: aspects of fluctuating lift. Journal of Fluids and Structures 15, 459–469.

Park, J., Kwon, K., Choi, H., 1998. Numerical solutions of flow past a circular cylinder at Reynolds numbers up to 160. KSME International Journal 12, 1200–1205.

Stojković, D., Breuer, M., Durst, F., 2002. Effect of high rotation rates on the laminar flow around a circular cylinder. Physics of Fluids 14, 3160–3178.

Sumner, D., Akosile, O.O., 2003. On uniform planar shear flow around a circular cylinder at subcritical Reynolds number. Journal of Fluids and Structures 18, 441–454.

Tamura, H., Kiya, M., Arie, M., 1980. Numerical study on viscous shear flow past a circular cylinder. Bulletin of the JSME 23, 1952–1958.

Tsien, H.S., 1943. Symmetrical Zhukovski airfoils in shear flow. Quarterly of Applied Mathematics 1, 130–148.

Williamson, C.H.K., 1989. Oblique and parallel modes of vortex shedding in the wake of a circular cylinder at low Reynolds numbers. Journal of Fluid Mechanics 206, 579–627.

Williamson, C.H.K., 1996. Vortex dynamics in the cylinder wake. Annual Review of Fluid Mechanics 28, 477–539.

Wu, T., Chen, C.-F., 2000. Laminar boundary-layer separation over a circular cylinder in uniform shear flow. Acta Mechanica 144, 71–82.

Yoshino, F., Hayashi, T., 1984. Numerical solution of flow around a rotating circular cylinder in uniform shear flow. Bulletin of the JSME 27, 1850–1857.

Zdravkovich, M.M., 1997. Flow around Circular Cylinders, vol. 1: Fundamentals. Oxford University Press, Oxford.